ACCMES 185

Heat engine activated by direct sunlight using shape memory alloy

Cheng Tang
School of Mechanical and Aerospace Engineering, Nanyang Technological University,
50 Nanyang Avenue, 639798, Singapore.
Email: tang0218@e.ntu.edu.sg
Wei Min Huang [#]
School of Mechanical and Aerospace Engineering, Nanyang Technological University,
50 Nanyang Avenue, 639798, Singapore.
Email: mwmhuang@ntu.edu.sg
[#] The corresponding author: Wei Min Huang

Abstract

Shape memory alloy (SMA) has been widely utilized in many applications especially as actuators due to its high actuation energy density. Heat engine is one typical example among them, which converts thermal energy into workable mechanical motions. In this paper, a prototype of SMA heat engine has been designed, fabricated, and characterized. Unlike those traditional prototypes which use hot fluid as the heating source for actuation, this novel five-beam offset crank heat engine could be driven by sunlight directly. Initially the prototype was observed to rotate at an average speed of 2 rpm under no external load, when efficiency was estimated. Influential factors that dominate the performance are investigated. It is suggested that using SMA with high transformation temperatures and small hysteresis, and accelerated cooling are effective ways to improve the efficiency. With optimization, the running speed could be increased up to 9 rpm.

Keywords: heat engine, shape memory alloy, sunlight, actuation, energy conversion.

1.Introduction

Shape memory alloy (SMA) is one type of smart material that is able to recover to its original shape upon suitable stimulus even if it is severely and quasi-plastically distorted before, which is a phenomenon known as the shape memory effect (SME) [1-3]. Due to the high actuation energy density it owns, SMA has already been utilized in many applications [4, 5]. Heat engine is one typical example among them, which converts thermal energy into mechanical energy. The idea has attracted investigations since many years ago, and various prototypes have been proposed so far [1, 6-9]. A typical offset crank engine uses several SMA actuators to connect a wheel and a crank that is offset from the wheel axis [9]. The differences in distance between edge of wheel and crank, together with differences in temperature trigger periodically phase transformation of SMA materials, leading to continuous rotation of wheel.

Despite of the differences in structure and mechanism, most SMA heat engines reported share one feature in common: they all use artificial hot fluid, either water or air, as the heating source to activate their motions. That might be the main restriction of SMA heat engine, since the maintenance of high temperature fluid itself is energy consuming, while the efficiency of energy conversion is quite low. It appears to be necessary to find an economic way to supply energy source before SMA heat engine could be put into broad-scale practical use. Geothermal energy seems to be one possible solution. However, suitable working location for this scheme is quite limited.

To overcome mentioned difficulties, a few schemes of utilizing light as the driving energy have been proposed. Some effect has been made to verify the feasibility of using laser to heat up pre-stretched SMA wires so as to lift weight [10], although the usage of high energy density laser is still a non-economic strategy. On the other hand, from engineering point of view, it is hoped that sunlight which is clean and available everywhere could be used as the energy source. Such heat engine will be completely environmental-friendly and have no restriction on working location. Simulation indicated that a SMA motor triggered by solar energy for space missions could have a maximum theoretic efficiency up to 9% [11]. The main concern is that whether sunlight, which has relatively lower energy density compared with other types of energy, is sufficient enough to activate SMA heat engine directly.

In this paper, we demonstrate a five-beam offset crank SMA heat engine that could be activated by sunlight directly. Although the working principle is similar with those prototypes in literature, this novel heat engine can run smoothly without any external power supply when exposed to the sun. Performances are recorded, and influential factors that determine the efficiency are characterized, together with further improvement proposed.

2.Design and fabrication

We have designed a prototype as schematically presented in Fig 1 and Fig 2, which are projected from top view and side view, respectively. Two discs with radius r_1 and r_2 ($r_1 > r_2$) are installed separately on two shafts, which are further eccentrically connected with an offset e. For each of five beams, two ends of the SMA actuator are fixed at the edge of these two discs (see point A and B shown in the illustrations) in a way that relative rotation between discs and SMA actuator is allowed. Obviously, the length of line $\overline{AB}$ l will vary at different positions due to the geometry structure. We define the angle between line $\overline{O_2A}$ and $\overline{O_2O_1}$ as the rotation angle α. When α equals to 0°, l will have the maximum value, as can be seen from Fig 1. Since the two discs are connected by SMA actuator, when one of them rotates, the other one would rotate correspondingly. It should be pointed out that these two discs will always have the same angular velocity as the result of equilibrium between all five beams. Therefore, the angle between line $\overline{O_1B}$ and $\overline{O_2O_1}$ also equals to α, as can be seen in Fig 1.

As the energy density of sunlight is below what is required to activate phase transformation of SMA, we use optical lenses to concentrate it. Transparent lenses supplied by Fresnel Technologies-Inc (USA) are used, the dimensions of which are 76×254 mm, 2 mm thickness and 76 mm focus length. From Fig 2, it can be seen that for each beam, a lens is placed right above the SMA actuator with a distance equals to focus length to ensure full concentration. The outer side of lens is clamped while the inner side could slide freely on the block supporting it. Bearings are embedded inside all connection points, i.e., A and B shown in Fig 1 and Fig 2, so that these blocks share the same freedom of rotation as the SMA actuator. Consequently, focused sunlight will fall on SMAs with accurate alignment at any instant. In this design, a maximum strain of 4% is used to balance the requirements of performance and life span. Corresponding geometric parameters are listed in Table 1.

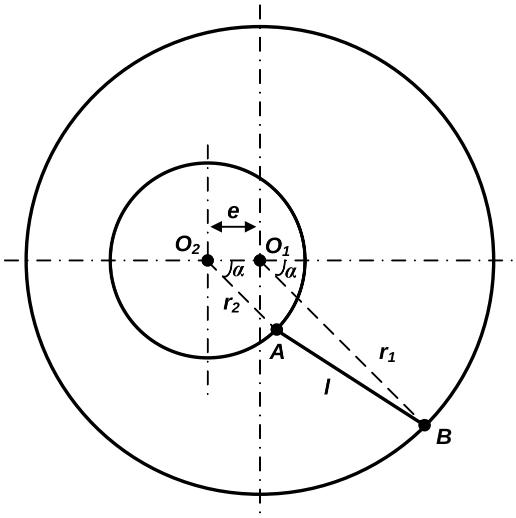

Fig 1. Geometric structure from top view. Not drawn in scale. For clear illustration, only one of the five beams is exhibited here. The other four beams have the similar setup. Black dots indicate bearings.

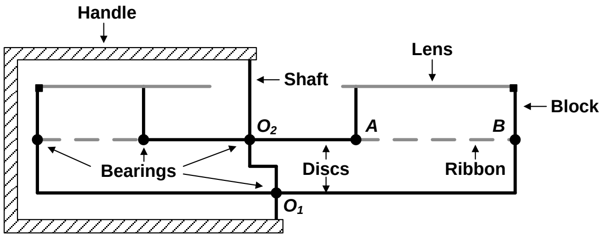

Fig 2. Geometric structure from side view. Not drawn in scale. Black dots indicate bearings.

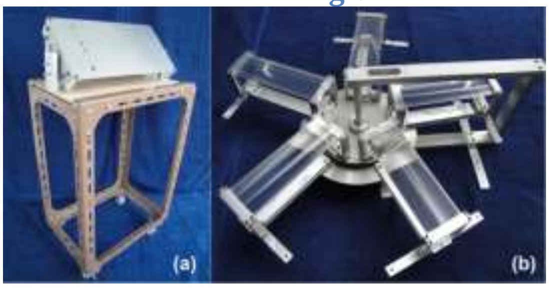

Fig 3. Fabricated prototype of sunlight activated SMA heat engine. (a) Adjustable platform with mobile supporting base; (b) main body of heat engine without cover.

Table 1 Geometric parameters of designed SMA heat engine

r_l	r_2	e	l
325 mm	100 mm	4.5 mm	220.5~229.5 mm

The fabricated prototype is exhibited in Fig 3. A mobile platform is used to adjust the angle in both horizontal and vertical plane so that the working plane of heat engine (i.e., plane of two discs) will always be perpendicular to the sunlight. Yet another external cover made of cardboard which is not shown here is used as blocker to sunlight. As a result, when one beam is exposed to the sunlight, the heated SMA actuator will contract and drive the whole heat engine; when it turns into the shadowed part, it will cool down and prevent the heat engine from rotating. Since the force generated by shape recovery is larger than that of tension resistance, the whole prototype can run continuously.

3.Experimental

The SMA actuators we have used are $Ni_{55.8}Ti_{44.2}$ ribbons, with cross-section 2×0.2 mm, provided by Mide Technology Corporation (USA). After heat-treatment at 500°C in an Elite 2416 furnace for one hour, good SME was observed in this material. A series of conventional tests were conducted to characterize the thermo-mechanical properties of used SMA materials. Differential scanning calorimeter (DSC) tests were carried out at a heating/cooling rate of 10°C/min on a TA Instruments DSC Q200. An Instron 5565 universal testing machine was used to conduct uniaxial tensile tests with loading/unloading rate of 0.05%/s at different temperatures.

The heat engine was placed in an open area at noon when it was sunny. The surrounding meteorological conditions were recorded as follows: ambient temperature: 30°C; relative humidity: 40%; sunlight intensity: 122×10^3 Lux. Only half of SMA heat engine is exposed to sunlight directly while the other half is sheltered by cardboard. No external load was applied. No slip of NiTi ribbon was observed throughout the whole experiment.

4.Results

Fig 4 shows the DSC results of used SMA ribbons. It is seen that three distinct phases, namely austenite, R-phase, and martensite will appear during one complete thermal cycle when no external stress is applied. Corresponding transformation temperatures, namely A_f, A_s, R_s, R_f, M_s, M_f, are 64°C, 49°C, 47°C, 40°C, 20°C, 7°C, respectively. Since the maximum tensile strain (4%) on NiTi ribbon is far beyond the elastic scope of R-phase, which is around 0.5% [12], it is most likely that all R-phase would transfer into martensite spontaneously and disappear during the thermo-mechanical cycle due to stress induced transformation. As such, we will consider two phases only, namely austenite and martensite, in the later discussion.

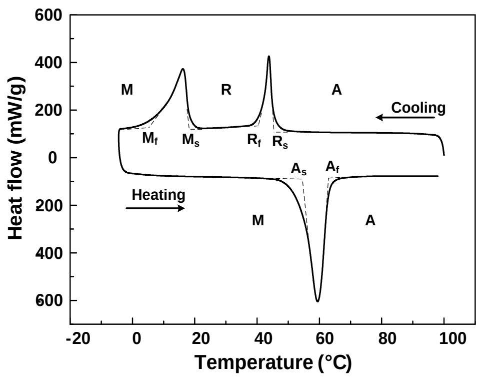

Fig 4. DSC result of Ni55.8Ti44.2 SMA in a stress free thermal cycle.

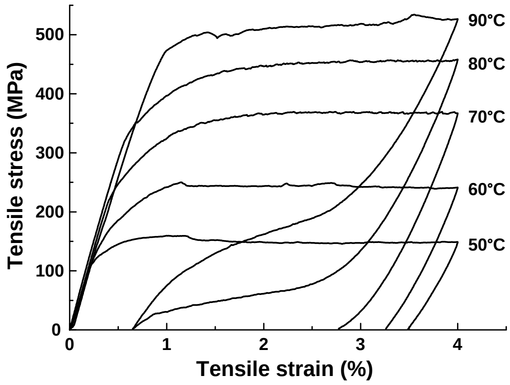

Fig 5. Stress vs. strain curves of NiTi ribbon in uniaxial stretching at different temperatures.

Fig 5 presents the experimental results of a series of uniaxial tensile tests in which a NiTi ribbon was stretched at different temperatures. It is noticed that after being stretched to over 1% strain, the measured stress becomes nearly a constant in all five curves, and the stabilized stress value increases with the rising of testing temperature in an approximately linear manner; while the residual strain after unloading drops significantly when temperature is increased. A large gap between the residual strains in tests conducted at 70°C and 80°C should be the result of martensite to austenite transformation above 70°C. When in austenite phase, SMA has the property of recovering almost all deformation, which is known as the super-elasticity or pseudoelasticity. It is also found that the transformation in a pre-stretched sample does not complete at 80°C. Even upon heating to 90°C, there is still a residual strain of about 0.65%. One possible explanation is that some interfaces between martensite and austenite may prevent the formation of other interfaces during the pseudoelastic process [13]. Therefore, stretched NiTi ribbons on this heat engine will not fully recover to their original shapes within the working temperature range.
At the given conditions, the heat engine was observed to rotate at an average speed of 2 rpm.

5.Discussions

The efficiency of the heat engine (η) can be defined as the ratio of output power (P_o) and input power (P_i). Since sunlight is the only energy source of this prototype, P_i is mainly determined by real time light intensity (I) and surface reflectivity of SMA (R_e). As light intensity and energy density are in two different units, we use a simple conversion formula based on definitions of both units, i.e., for sunlight, every 251 Lux measured is roughly considered as 1 W/m^2 [14]. Due to the reflection, there is immediate energy loss and only a small portion of focused sunlight contributes to the heating of NiTi ribbon. Hence the input power can be expressed as:

$$P_i = I \times S_L \times (1 - R_e) / 251 \quad (1)$$

where S_L is the area of one lens.

Heat dissipation always exists when heat engine is at work. Convection and radiation are the two major forms of heat dissipation in this case, while conduction is negligible because of the small contact area between NiTi ribbons and fixture. According to classic heat transfer theory, the power loss due to convection (P_c) and radiation (P_r) are:

$$P_c = S_R \times h \times (T - T_\infty) \quad (2)$$

$$P_r = S_R \times E \times \sigma \times (T^4 - T_\infty{}^4) \quad (3)$$

where S_R is the surface area of NiTi ribbon, h is the free convection coefficient, T is the temperature of NiTi ribbon in Kelvin, T_∞ is the ambient temperature in Kelvin, E is the emissivity, σ is the Stefan-Boltzmann constant.

When the heat engine is running stably, NiTi ribbon installed on each beam goes through reversible transformations between highest working temperature (T_H) and lowest temperature (T_L) periodically. Since time for heating and cooling part in one full cycle is roughly even (half of heat engine is sheltered from light), each of them is around 15 seconds given the average speed of 2 rpm. As such, T_H and T_L should satisfy the following conditions: during heating there is:

$$\int_0^{15} (P_i - P_c - P_r) dt = V \times \rho \times [c \times (T_H - T_L) + q_M + q_D] \quad (4)$$

and for cooling:

$$\int_0^{15} (P_c + P_r) dt = V \times \rho \times [c \times (T_H - T_L) + q_M - q_D] \quad (5)$$

where V is the volume of NiTi ribbon, ρ is the mass density of NiTi ribbon, c is the heat capacity of NiTi ribbon, q_M is the latent heat for martensite to austenite transformation derived from DSC result, q_D is the energy dissipation during martensite to austenite transformation derived from DSC result.

In the calculation, a small time step (dt) is applied, and the corresponding little temperature change is added into the previous result to get a new start temperature for the next time step. Thermal expansion of SMA is ignored in all calculations since its contribution is relatively small. The SMA material experiences only 80% phase transformation during both heating and cooling, leaving the rest 20% unchanged as martensite all the time, which is confirmed by the uniaxial tensile test. By using the parameters in Table 2, we can work out T_H and T_L as 79.0°C and 48.8°C, respectively. It should be pointed out that the SMA heat engine is self-adaptive with external conditions, such as light intensity, shadowed area, and applied load, etc. Therefore, T_H and T_L may vary under different testing conditions. For this particular case, the temperature of SMA at any time could be simulated as shown in Fig 6. The turning point at both heating and cooling curve marks the start of phase transition.

Table 2 Parameters for calculation of efficiency

I	S_L	S_R	R_e	h

122×10^3 Lux	1.71×10^{-2} m^2	4.5×10^{-4} m^2	80.5%	10
T_∞	E	σ	V	ρ
303 K	0.74 [15]	5.67×10^{-8} W/m^2·K^4	9×10^{-8} m^3	6.45×10^3 kg/m^3
c	q_M	q_D		
322 J/kg·°C	14.4 J/g	2.6 J/g		

We will then use stress-strain curve to simulate the output torque that each beam can generate during one cycle. Strictly speaking, at least four factors, i.e. stress, strain, time, and temperature, should be considered simultaneously to study this dynamic process in SMA heat engine. Simplifications are applied here to work out the first order estimation. Using the rotation angle α defined previously, we can work out the curve of torque at any angle as shown in Fig 7. A positive torque between 0° and 180° is the driving torque generated by the recovery stress upon heating by sunlight; while a negative torque between 180° and 360° is the resistant torque generated by the tensile stress in NiTi ribbon during stretching. With integration, the average output power P_o can be calculated to be 0.0137 W. While the input power P_i is derived from Eqn (1) as 4.05 W, the efficiency of this SMA heat engine under zero load is then 0.338%.

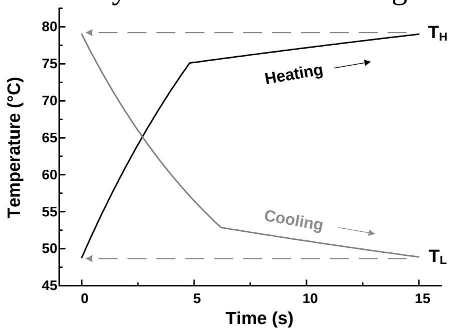

Fig 6. Temperature change in SMA during one full cycle.

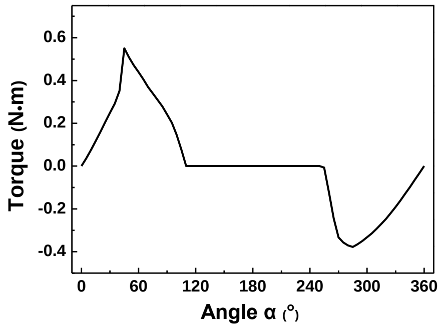

Fig 7. Relationship between rotation angle *α* and torque.

The output power under loading should be obtained through actual measurement, which is expected to be a function of the applied load. Due to the limited condition, e.g., the intensity of sunlight is always changing, no reliable experimental result of the real output power under loading is obtained so far. It is believed that the efficiency will increase to a higher value when a certain amount of load is applied. To compare, a few theoretical models studying the efficiency of conventional SMA heat engines have been proposed [16-19]. Reported maximum efficiency varies from less than 2% to 26%. For prototypes that have been constructed so far, the efficiency, if mentioned, is around 1% at most [6].

Two main factors restrict the efficiency of this SMA heat engine. One is the thermo-mechanical properties of SMA itself. It is self-evident that a higher elastic modulus of material will lead to a larger output torque thus the efficiency. So does a smaller hysteresis of SMA. This is because the heating process does not contribute to any phase transition other than raising the material temperature until it reaches A_s, therefore no output work is done during this period of time. However, energy is always dissipating by means of convection and radiation, which causes the low efficiency. Moreover, compared with heating, cooling part is more difficult to control as the only approach is through natural heat transfer. It is then hoped that the phase transitions occur at higher temperature range, so that a larger temperature gap between object and ambient helps to generate higher cooling rate, as can be seen from Eqn (2) and (3). As such, SMA with high A_f and A_s is required.

Another factor is about accelerated cooling. In a forced cooling condition, the convection coefficient h could be as high as 50~100, compared with currently used 10, which would increase the cooling rate significantly. In practice, another effective and convenient approach is to adjust covered area of heat engine. According to Fig 7, when rotation angle α is over 120°, the driving torque is already attenuated to zero and provides no contribution to the running of heat engine, although the ribbon is still under heating. Therefore, we can increase the covered ratio to 2/3 to fully utilize the driving torque and provide more time for the ribbon to be cooled down, thus resistant torque is reduced accordingly.

An experiment was conducted with 2/3 covered ratio and forced cooling using an electrical fan. Other meteorological conditions were the same as former one. In the experiment, the position and blow direction of the fan were carefully adjusted to avoid causing any additional motion to the engine. This was verified by the fact that no motion was observed when the heat engine was put indoor and blown by electrical fan only, with no sunlight irradiated. The average speed was observed to increase to 9 rpm. This result clearly demonstrated that the efficiency has been improved after optimizations.

6.Conclusions

We present a novel SMA heat engine that directly utilizes sunlight to drive its motion. Sunlight is concentrated on NiTi ribbons through optic lenses, thus heats the ribbons to induce the SME which drives the continuous motion of the engine. A prototype has been designed, fabricated and characterized. Efficiency of this heat engine is investigated. Major factors that affect the performance of such heat engine are discussed. After optimization, a maximum average speed of 9 rpm is achieved from original 2 rpm in this particular prototype. Such model is expected to have various applications especially in space missions, being one alternative to solar cell.

References

[1] H. Funakubo, editor Shape Memory Alloys. New York: Gordon and Breach Science Publishers, 1987.

[2] W.M. Huang, Z. Ding, C.C. Wang, J. Wei, Y. Zhao, H. Purnawali. Shape memory materials. *Materials Today* 13 (2010) 54-61.

[3] K. Otsuka, C.M. Wayman, editors. Shape Memory Materials. Cambridge: Cambridge University Press, 1998.

[4] D.C. Lagoudas, editor Shape Memory Alloys Modeling and Engineering Applications. New York: Springer Science+Business Media, LLC, 2008.

[5] L. Sun, W.M. Huang, Z. Ding, Y. Zhao, C.C. Wang, H. Purnawali, C. Tang. Stimulus-responsive shape memory materials: A review. *Materials & Design* 33 (2012) 577-640.

[6] R. Salzbrenner. Shape memory heat engines. *Journal of Materials Science* 19 (1984) 1827-1835.

[7] A.P. Jardine. A shape memory effect swashplate heat engine. *Materials Letters* 7 (1988) 102-105.

[8] E.H. Schiller. Heat engine driven by shape memory alloys: prototyping and design. Master dissertation. Blacksburg, VA: Virginia Polytechnic Institure and State University, 2002.

[9] W.S. Ginell, J.L. McNichols Jr, J.S. Cory. Nitinol heat engines for low-grade thermal energy conversion. *Mechanical Engineering* 101 (1979) 28-33.

[10] H. Okamura, K. Yamaguchi, R. Ono. Light-driven actuator with shape memory alloy for manipulation of macroscopic Objects. *International Journal of Optomechatronics* 3 (2009) 277-288.

[11] X.Y. Gao, W.M. Huang. Shape memory motor directly powered by solar energy for space missions. *Proceedings of the 2006 IEEE International Conference on Mechatronics and Automation*, vol. 2006. Luo yang, 2006. p.243-248.

[12] K. Otsuka. Introduction to the R-phase transition. In *Engineering Aspects of Shape Memory Alloys*. Butterworth-Heinemann, 1990. p.36-45.

[13] T.W. Shield. Orientation dependence of the pseudoelastic behavior of single crystals of CuAlNi in tension. *Journal of the Mechanics and Physics of Solids* 43 (1995) 869-895.

[14] A. Stimson. Photometry and Radiometry for Engineers. New York: John Wiley & Sons Inc, 1974.

[15] J. Zurbitu, S. Kustov, A. Zabaleta, E. Cesari, J. Aurrekoetxea. Thermo-mechanical behaviour of NiTi at impact. In: C. Cismasiu, editor. *Shape Memory Alloys*. Rijeka: Sciyo, 2010.

[16] P.G. McCormick. On the practical efficiency of shape memory engines. *Scripta Metallurgica* 21 (1987) 99-101.

[17] A. Ziótkowski. Theoretical analysis of efficiency of shape memory alloy heat engines (based on constitutive models of pseudoelasticity). *Mechanics of Materials* 16 (1993) 365-377.

[18] J.J. Zhu, N.G. Liang, W.M. Huang, K.M. Liew. Energy conversion in shape memory alloy heat engine Part II: Simulation. *Journal of Intelligent Material Systems and Structures* 12 (2001) 133-140.

[19] M.A. Thrasher, A.R. Shahin, P.H. Meckl, J.D. Jones. Efficiency analysis of shape memory alloy actuators. *Smart Materials and Structures* 3 (1994) 226-234.